AMERICAN JOURNAL OF PHYSIOLOGY
CELL PHYSIOLOGY

Am J Physiol Cell Physiol 324: C757–C768, 2023.
First published February 6, 2023; doi:10.1152/ajpcell.00288.2022

RESEARCH ARTICLE

Functional maturation of kidney organoid tubules: PIEZO1-mediated Ca^{2+} signaling

Rolando Carrisoza-Gaytan,[1] Katharina T. Kroll,[2] Ken Hiratsuka,[2,3,4] Navin R. Gupta,[3,4] Ryuji Morizane,[2,3,4,5] Jennifer A. Lewis,[2,5] and Lisa M. Satlin[1]

[1]*Department of Pediatrics, Icahn School of Medicine at Mount Sinai, New York, New York, United States;* [2]*Paulson School of Engineering and Applied Sciences, Wyss Institute for Biologically Inspired Engineering, Harvard University, Cambridge, Massachusetts, United States;* [3]*Nephrology Division, Massachusetts General Hospital, Boston, Massachusetts, United States;* [4]*Department of Medicine, Harvard Medical School, Boston, Massachusetts, United States; and* [5]*Harvard Stem Cell Institute, Cambridge, Massachusetts, United States*

Abstract

Kidney organoids cultured on adherent matrices in the presence of superfusate flow generate vascular networks and exhibit more mature podocyte and tubular compartments compared with static controls (Homan KA, Gupta N, Kroll KT, Kolesky DB, Skylar-Scott M, Miyoshi T, Mau D, Valerius MT, Ferrante T, Bonventre JV, Lewis JA, Morizane R. *Nat Methods* 16: 255-262, 2019; Takasato M, Er PX, Chiu HS, Maier B, Baillie GJ, Ferguson C, Parton RG, Wolvetang EJ, Roost MS, Chuva de Sousa Lopes SM, Little MH. *Nature* 526: 564-568, 2015.). However, their physiological function has yet to be systematically investigated. Here, we measured mechano-induced changes in intracellular Ca^{2+} concentration ($[Ca^{2+}]_i$) in tubules isolated from organoids cultured for 21–64 days, microperfused in vitro or affixed to the base of a specimen chamber, and loaded with fura-2 to measure $[Ca^{2+}]_i$. A rapid >2.5-fold increase in $[Ca^{2+}]_i$ from a baseline of 195.0 ± 22.1 nM (n = 9; $P \leq 0.001$) was observed when microperfused tubules from organoids >40 days in culture were subjected to luminal flow. In contrast, no response was detected in tubules isolated from organoids <30 days in culture. Nonperfused tubules (41 days) subjected to a 10-fold increase in bath flow rate also exhibited a threefold increase in $[Ca^{2+}]_i$ from baseline ($P < 0.001$). Mechanosensitive PIEZO1 channels contribute to the flow-induced $[Ca^{2+}]_i$ response in mouse distal tubule (Carrisoza-Gaytan R, Dalghi MG, Apodaca GL, Kleyman TR, Satlin LM. *The FASEB J* 33: 824.25, 2019.). Immunodetectable apical and basolateral PIEZO1 was identified in tubular structures by 21 days in culture. Basolateral PIEZO1 appeared to be functional as basolateral exposure of nonperfused tubules to the PIEZO1 activator Yoda 1 increased $[Ca^{2+}]_i$ ($P \leq 0.001$) in segments from organoids cultured for >30 days, with peak $[Ca^{2+}]_i$ increasing with advancing days in culture. These results are consistent with a maturational increase in number and/or activity of flow/stretch-sensitive Ca^{2+} channels, including PIEZO1, in tubules of static organoids in culture.

development; fluid flow; mechanoregulation; microperfusion; signal transduction

INTRODUCTION

Both intrinsic and extrinsic mechanical forces play critical roles in tissue morphogenesis and homeostasis during development (reviewed in Refs. 1–6). Kidney organoids differentiated from human pluripotent stem cells under static conditions are relatively immature at *day 25* of culture compared with their terminally differentiated adult counterparts (7–9). Specifically, they possess limited vasculature and their gene expression profiles of tubular epithelia are akin to a first or second-trimester kidney (7). However, when these organoids are cultured in the presence of superfusate (bath) flow, a pervasive microvasculature develops with a concomitant enhancement in the maturity of podocyte and tubular compartments, as demonstrated by improved cellular polarity and adult gene expression compared with static controls (10).

We and others have shown that increases in luminal flow rate subject epithelial cells in the fully differentiated mammalian distal nephron to apical fluid shear stress (FSS), circumferential stretch (CS) of both apical and basolateral membranes, and drag and torque on apical cilia and microvilli (11, 12). These forces are transduced into biphasic increases in $[Ca^{2+}]_i$ in renal epithelial cells. An initial rapid increase in $[Ca^{2+}]_i$ to a peak value within ~10 s reflects extracellular Ca^{2+} entry at the basolateral membrane coupled with release of IP_3-sensitive internal Ca^{2+} stores (11). In the adult rabbit or mouse, the peak $[Ca^{2+}]_i$ transient is followed by a decay to a plateau elevation in $[Ca^{2+}]_i$, sustained throughout the period of high flow, reflecting luminal Ca^{2+} entry that is, in part, mediated by transient receptor potential vanilloid 4 (TRPV4) channels (11, 13–17). Distal nephron segments isolated from neonatal mice demonstrate a typical flow-induced

Correspondence: L. M. Satlin (lisa.satlin@mssm.edu).
Submitted 30 June 2022 / Revised 25 January 2023 / Accepted 26 January 2023

peak in $[Ca^{2+}]_i$ that increases in amplitude over the first 2 wk of postnatal life, but fail to exhibit a sustained plateau elevation in $[Ca^{2+}]_i$ in the continuous presence of flow during this interval (18, 19).

Piezo channels are mechanoactivated, nonselective cation channels that have been proposed to function as mechanosensors (20–25). In isolated mouse proximal tubule cells, Piezo1 mediates a mechanosensitive ion current (26), and in urothelium, mechanosensitive Ca^{2+} influx and ATP release (27). Notably, PIEZO1 has been reported to be required for proper vascular development and cell rearrangements in response to flow in mouse (28–30). PIEZO1 is also required for stretch-triggered epithelial proliferation and crowd sensing (31). PIEZO channels are critical in development, as global *Piezo1* or *Piezo2* KO mice die during embryogenesis or at birth, respectively (29, 30, 32). Ca^{2+} signaling mediated by the single Piezo homolog in Drosophila stimulates proliferation and differentiation in the gut, albeit through distinct pathways: ERK phosphorylation and Notch inhibition, respectively (33). Importantly, PIEZO1 is expressed along the basolateral membranes of renal tubular epithelial cells in the mouse kidney (34), an ideal location to sense extrinsic FSS.

Given the role of Piezo channels in development and Ca^{2+} signaling to a key pattern forming events during early vertebrate development (35–37), we sought to characterize the *1*) mechanoinduced Ca^{2+} responses to increases in luminal or basolateral flow and *2*) expression of PIEZO1 in tubular structures microdissected from maturing static kidney organoids. This study is the first to apply the technique of in vitro microperfusion to kidney organoid tubules to demonstrate the developmental regulation of mechanosensitive Ca^{2+} signaling in cells therein.

METHODS

Kidney Organoid Generation, Differentiation, and Culture

H9 (WiCell) female human embryonic stem cells (hESCs) and BJFF male human iPS cells (provided by S. Jain at Washington University) were maintained on hESC-qualified Geltrex (Thermo Fisher Scientific) coated plates using StemFit Basic02 (Ajinomoto Co., Inc.) supplemented with 10 ng/mL of FGF2 (Peprotech), as previously reported (38). The H9 hESCs were passaged weekly, using Accutase (STEMCELL technologies) for dissociation and Y27632 (Tocris) to facilitate adhesion on passaging.

The directed differentiation of hPSCs into kidney organoids is covered in detail elsewhere (38, 39). Briefly, hPSCs were differentiated into nephron progenitor cells (NPCs), with ~80%–90% efficiency, by a three-step-directed differentiation protocol. NPCs, arising on *day 8* of differentiation, were transferred into suspension culture in 96-well ultralow adhesion plates (Corning) and followed for further differentiation into kidney organoids through intermediate stages of pretubular aggregates (*day 11*) and renal vesicles (*day 14*), as previously reported (38, 39). Kidney organoids were maintained in 200 μL of basal media consisting of Advanced RPMI (ARPMI, Thermo Fisher) and 1× GlutaMAX (Thermo Fisher) in 96-well plates following induction of renal vesicles at *day 14* of differentiation. Media changes were conducted three times weekly with removal of 95 μL and addition of 100 μL of fresh basal media until the day of experimentation. Organoids cultured for >21 days were transported over 4–5 h at room temperature (RT) from the Massachusetts General Hospital to the Icahn School of Medicine at Mount Sinai. On arrival, they were immediately placed in an incubator at 5% CO_2 and 37°C for continuation of culture.

Kidney Organoid Quality Control

Several metrics are used to assess kidney organoid quality, including immunostaining for the NPC marker, SIX Homeobox 2 (SIX2), on differentiation *day 8* and Cadherin 1 (CDH1), Lotus tetragonolobus lectin (LTL), and Podocalyxin Like (PODXL) on *day 21* using antibodies previously validated by for specificity (39). Table 1 provides details for antibodies used. For SIX2 immunostaining in 24 well plates, samples were washed with phosphate-buffered saline (PBS) and fixed for 30 min with 250 μL of 4% paraformaldehyde (PFA, Electron Microscopy Sciences). Samples were washed with 1-mL PBS three times to remove the fixative, blocked using 5% donkey serum in PBS containing 0.3% TritonX-100 for 1 h, and then washed with PBS three times. Samples were then incubated with SIX2 primary antibody (Proteintech, 11562-1-AP, DF 1:500) in antibody diluting buffer (ADB; 1% BSA, 1× PBS, 0.3% TritonX-100) for 1 h at RT, or overnight at 4°C, then washed with PBS three times. Next, samples were incubated with Alexa Fluor secondary antibody in ADB for 1 h at RT and washed with PBS three times. Samples were counterstained with a 1:5,000 solution of DAPI (4,6-diamidino-2-phenylindole; Vector Laboratories) diluted in PBS and imaged using Leica Stellaris 8 with image rendering via free LAS-X software. For CDH1, LTL, and PODXL whole mount immunostaining in suspension culture, three organoids per plate were transferred to 1.5-mL Eppendorf tubes, washed with PBS, then fixed for 1 h while submerged in 250 μL of 4% PFA, and washed with PBS three times. Samples were incubated with primary antibodies (Table 1) directed at CDH1, LTL-biotin, and PODXL diluted in 250 μL of ADB overnight at 4°C. Samples were then washed with PBS three times and incubated with Alexa Fluor secondary antibodies in ADB for 1 h at RT, before washing with PBS three times. Samples were counterstained with DAPI and imaged using Leica Stellaris 8 with image rendering via free LAS-X software. We carried out SIX2 and CDH1, LTL, and PODXL immunostaining on all batches of kidney organoids to ensure nephron induction and limit batch-to-batch heterogeneity.

Microdissection and In Vitro Microperfusion of Isolated Organoid Tubules

A single organoid was placed in chilled dissection solution containing (in mM): 145 NaCl, 2.5 K_2HPO_4, 2.0 $CaCl_2$, 1.2 $MgSO_4$, 4.0 Na lactate, 1.0 Na citrate, 6.0 L-alanine, and 5.5 glucose (pH 7.4, 290 ± 2 mosmol/kgH_2O). Single tubule segments (0.1–0.3 mm length) were isolated by manual dissection within 60 min and transferred to a temperature and O_2/CO_2-controlled specimen chamber assembled with a No. 1 coverslip (Corning) painted with a 1-μL drop of poly-D-lysine hydrobromide 0.01% (BD Biosciences, Bedford, MA). The specimen chamber was set on the stage of the Nikon Eclipse TE 300 inverted epifluorescence microscope linked to a Zyla

Table 1. *Antibodies used for immunolabeling*

1° Antibody	Final Concentration	Company	Cat. No.	2° Antibody	Final Concentration	Company	Cat. No.
Rabbit anti-Piezo1	5 μg/mL	Sigma-Aldrich	HPA047185	Atto-549-goat anti-rabbit IgG	4 μg/mL	Sigma-Aldrich	77671
				Alexa Fluor-555 donkey anti-rabbit IgG	4 μg/mL	Invitrogen	A31572
Mouse IgG2b anti-acetylated α-tubulin	2 μg/mL	Abcam	ab24610	A488-goat anti-mouse IgG	2 μg/mL	Molecular Probes	A11029
Mouse IgG2a anti-actin	10 μg/mL	Sigma-Aldrich	A3853				
human IgG anti-PODXL	10 μg/mL	R&D	AF1658	Alexa Fluor-647 donkey anti-goat IgG	4 μg/mL	Invitrogen	A21447
Rat IgG1 anti-E-CDH1	2 μg/mL	Abcam	ab11512	Alexa Fluor-594 donkey anti-rat IgG	4 μg/mL	Invitrogen	A21209
LTL (lectin)	10 μg/mL	Vector Lab	B-1325	Alexa Fluor-750 streptavidin conjugate	2 μg/mL	Invitrogen	S21384
Rabbit IgG anti-SIX2	1.5 μg/mL (assuming stock is 750 μg/mL)	Proteintech	11562-1-A	Alexa Fluor-488 donkey anti-rabbit IgG	2 μg/mL	Invitrogen	A21206
Piezo1 antigen	60 μg/mL	Sigma-Aldrich	APREST71755				
DAPI		Sigma-Aldrich	D8417				

4.2 sCMOS camera (ANDOR Technology), interfaced with a digital imaging system (MetaFluor, Universal Imaging, Westchester, PA). Each isolated tubule was positioned directly on the poly-D-lysine to immobilize the segment for the duration of the experiment.

In vitro microperfusion studies were performed using standard methodology, as previously described (40, 41). Briefly, the tubule was cannulated on concentric glass pipettes at one end only for luminal perfusion and perfused and bathed in Burg's solution containing (in mM): 120 NaCl, 25 $NaHCO_3$, 2.5 K_2HPO_4, 2.0 $CaCl_2$, 1.2 $MgSO_4$, 4.0 Na lactate, 1.0 Na_3 citrate, 6.0 L-alanine, and 5.5 D-glucose, pH 7.4, 290 ± 2 mosmol/kgH_2O. Nonperfused segments affixed to the coverslip were also bathed in Burg's perfusate. Following a 1 h equilibration, during which time the perfusion chamber was continuously suffused with a gas mixture of 95% O_2-5% CO_2 to maintain pH at 37°C, segments were loaded with 20 μM of the acetoxymethyl ester of fura2 (fura 2-AM; Calbiochem, La Jolla, CA) added to the bath for 20 min. Each tubule was then rinsed with perfusate for 30 min. The bathing solution was continuously exchanged at a rate of 10 mL/h, unless otherwise indicated, using a syringe pump (Razel, Stamford, CT).

Measurement of Intracellular Ca^{2+} Concentration ($[Ca^{2+}]_i$)

Fura-2-loaded segments were alternately excited at 340 nm and 380 nm and images, acquired every 3 s, were digitized for subsequent analysis, as previously described (40, 41). After stable baseline 340 nm/380 nm fura-2 fluorescence intensity ratios (FIRs) were obtained, luminal or bath flow rate was increased as indicated, or Yoda1 [2-(5-{[(2,6-Dichlorophenyl)methyl]sulfanyl}-1,3,4-thiadiazol-2-yl)pyrazine], a synthetic small molecule that binds to and activates the Piezo1 channel from the intracellular side of the membrane (23, 42), was added to the bathing solution of nonperfused segments. One subset of nonperfused tubules was pretreated with the nonselective Piezo inhibitor Grammostola Mechanotoxin No. 4 (GsMTx4, 5 μM) (43) before exposure to an increase in bath flow rate. GsMTx4 incorporates into the cell membrane, distorting the distribution of tension near the channel, thereby inhibiting the response of the channel to mechanoactivation (44).

FIRs were subsequently monitored using a commercially available digital image analysis system (MetaFluor, Molecular Devices). At the conclusion of most experiments, an intracellular calibration was performed, using 10 μM EGTA-AM in a Ca^{2+}-free bath and then a 2 mM Ca^{2+} bath containing ionomycin (10 μM) (45). Standard equations were used to calculate experimental values of $[Ca^{2+}]_i$. Because we sought to confirm cell viability by trypan blue exclusion at the conclusion of Yoda1 dose-response assays, we elected to report only FIRs and not absolute measurements of $[Ca^{2+}]_i$, which would have required exposure to tubules to ionomycin and high Ca^{2+} for calibration. In general, at least three randomly chosen cells, devoid of adherent nonepithelial cells, were analyzed in the wall of each tubule.

Immunolocalization of PIEZO1

To examine PIEZO1 localization within maturing organoids, a subset of organoids labeled with PODXL (glomerular podocyte marker), LTL (proximal tubule marker) and CDH1 (loop of Henle and distal tubule marker) were labeled with our rabbit anti-PIEZO1 antibody (see Table 1 for all antibody dilutions) overnight at 4°C and secondary Atto549-conjugated goat anti-rabbit IgG (Table 1) for 1 h at RT. For peptide competition experiments, 60 μg of peptide was added to 5 μg of the primary PIEZO1 antibody in 1 mL of antibody solution (containing 0.1% BSA, 1% goat serum, and 0.1% Triton X-100 in PBS), preincubated at RT for 2 h and then spun down. Tissue was incubated with the supernatant overnight at 4°C, following the immunolabeling protocol summarized below.

To examine PIEZO1 localization within maturing tubules, 10-μm cryosections were cut from organoids that had been cryoprotected in 30% sucrose (in PBS) overnight at 4°C and subsequently embedded in Tissue-Tek OCT compound before freezing in liquid nitrogen. Tissue sections were placed on a glass slide and stored at −20°C until use. Sections were defrosted to RT and rehydrated with 137 mM NaCl, 2.7 mM KCl, 8 mM Na_2HPO_4, and 2 mM KH_2PO_4 (pH 7.4; PBS), permeabilized with 0.1% Triton X-100 in PBS for 10 min, and blocked

with a solution containing 1% BSA, 10% goat serum, and 0.1% Triton X-100 in PBS at RT for 1 h. All antibody sources and final concentrations are summarized in Table 1. Sections were then incubated sequentially with a rabbit anti-PIEZO1 antibody overnight at 4°C and secondary Atto549-conjugated goat anti-rabbit IgG for 1 h at RT in antibody solution. Sections were then colabeled with specific primary antibodies and appropriate fluorescent secondary antibodies to identify actin or anti-acetylated α-tubulin (Table 1). Nuclei were counterstained with DAPI (1 μg/mL for 5 min at RT), washed three times with PBS (5 min per wash at RT), and mounted with Vectashield antifade mounting medium (Vector Labs, H-1200, Vector Labs). Sections were then directly visualized by confocal microscopy using a ×10 air (NA 0.4) or ×63 oil-immersion plan-Apochromat objective (NA 1.4) and a laser-scanning Leica SP5 DM. Stacks of confocal sections were collected using a pinhole of 65.3 μm and step size of 1 μm. 3 D reconstructions and analysis of FIRs were performed using Leica Application Suite (LAS-X) software.

Bulk RNA-Seq of Kidney Organoids

The bulk RNA-seq data used here was derived from a previously reported dataset (46). Briefly, total RNA was isolated from kidney organoids on differentiation *days 8*, *21*, *35*, *49*, and *63* using Trizol (Thermofisher), following the manufacturer's protocol. RNA integrity was assessed by RNA Nano 6000 Assay Kit and Bioanalyzer 2100 (Agilent Technologies, CA). Each 400 ng total RNA was used for library preparation using NEBNext Ultra II RNA Library Prep Kit for Illumina (New England BioLabs, #E7775). The resulting library was quantified using Qubit for mass concentration, LabChip for fragments distribution, and qPCR for molar concentration. The qualified RNA-seq libraries were run on Novaseq 6000 S4 sequencers (Illumina). Downstream analysis was performed using a combination of programs, including Spliced Transcripts Alignment to a Reference (STAR; v2.5), HTseq (v0.6.1), Cufflink and our wrapped scripts. Reference genome and gene model annotation files were downloaded from genome website browser (NCBI/UCSC/Ensembl) directly. Indexes of the reference genome were built using STAR and paired-end clean reads were aligned to the reference genome using STAR (v2.5). The accession number for the bulk RNA sequencing data reported is DDBJ Sequence Read Archive (DRA):DRA010266.

RT-qPCR

RNA was isolated from kidney organoid samples using TRIzol (Invitrogen) following the manufacturer's protocol. A minimum of three and a maximum of six organoids were used per sample. cDNA was synthesized from 500 ng of RNA using a High-capacity cDNA Reverse Transcription kit (Applied Biosystems). Quantitative real-time PCR (qPCR) was performed using iTaq SYBR green supermix (Bio-Rad) and a Bio-Rad iQ5 Multicolor Real-time PCR Detection System. Primer sequences (Table 2) were designed using FASTA sequences (PubMed) and verified using Primer3, with one primer from each primer pair being designed to include an exon-exon junction to limit the effect of potential residual genomic DNA. Primer-BLAST (NCBI) confirmed the specificity of the primer pairs. Target genes were normalized to expression of glyceraldehyde 3-phosphate dehydrogenase (GAPDH). The mRNA expression was calculated using the $2^{-}\Delta^{\Delta Ct}$ method, expressed as an *n*-fold difference relative to the control group (*day 8*).

Statistical Analysis

Each experiment was performed using at least three organoids per group, unless specifically indicated. All results are expressed as mean ± SD. An unpaired two-tailed Student's *t* test was used to compare differences between days in culture, whereas a paired Student's *t* test was used to compare differences between data collected in a single tubule segment. For multiple comparisons, ANOVA was used; posttest details are provided in the figure legends. Statistical significance was taken as $P < 0.05$.

RESULTS

Luminal Flow-Induced $[Ca^{2+}]_i$ Response Is Enhanced in Microperfused Tubules Isolated from Kidney Organoids Cultured Longitudinally

Microdissected organoid tubules appeared to end in a blind pouch, yet their epithelial cells were easily distinguishable and lined what appeared to be closed lumens (Fig. 1). Tubules were cannulated from the "closed end" (to enable flow through the lumen) and perfused in a retrograde direction. Our observation that tubules isolated from organoids as early as 21 days in culture and incubated in cell-permeant fura-2 AM concentrated the ratiometric indicator dye indicates the presence of cellular esterases necessary to remove the AM moiety (45) in organoids at all developmental stages studied. Note that we could not determine whether microdissected isolated tubules were proximal or distal.

Baseline $[Ca^{2+}]_i$ did not differ among H9 organoids cultured for 21–60 days under identical conditions, averaging 194.5 ± 32.7 nM (n = 18 tubules from 18 organoids; Table 3), a value greater than that reported for neonatal and adult proximal tubule (47) and collecting duct (19) in rodent. A rapid increase in $[Ca^{2+}]_i$ was observed when tubules isolated from organoids >40 days in culture were subjected to an acute increase in luminal flow (anticipated to lead to apical FSS, CS with deformation of the apical and basolateral membranes,

Table 2. *Primer sequences*

Gene	Forward Primer	Reverse Primer
ACTB	CTCTTCCAGCCTTCCTTCCT	AGCACTGTGTTGGCGTACAG
GAPDH	CAATGACCCCTTCATTGACC	GACAAGCTTCCCGTTCTCAG
PIEZO1	ATGTTGCTCTACACCCTGACC	CCAGCACACACATAGATCCAGT
PMCA1	AGCAGTTATGTGGGGACGAA	GCCTTAAGCGGTGAGTCTTGA
TRPV4	CTACGGCACCTATCGTCACC	TTAGGCGTTTCTTGTGGGTCA

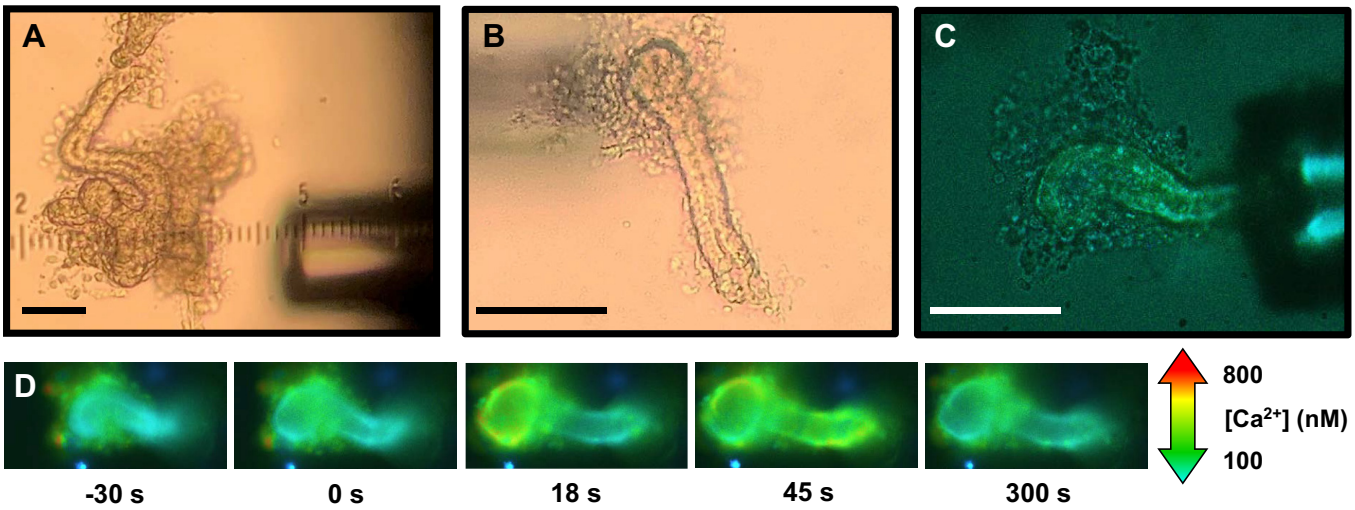

Figure 1. In vitro microperfusion of tubules isolated from static kidney organoids. Light microscopic appearance of single tubular structures microdissected from 59-day (*A*) and 57-day (*B*) organoids cultured under static conditions. *C*: the same tubule (~40 mm in diameter) shown in *B*, held securely in a microperfusion micropipette (right), was cannulated, perfused, loaded with 20 μM fura-2 and then filled with perfusate to open the tubular lumen. *D*: in response to hydrodynamic forces elicited by luminal filling, cell Ca^{2+} concentration ($[Ca^{2+}]_i$) increased over time, demonstrated by the change from blue to green pseudocolor (corresponding to an increase in the 340 nm/380 nm fluorescence intensity ratio), in both the tubule shaft and blind distal pouch. Bars in *A*, *B*, and *C* = 100 μm.

and drag/torque on apical cilia and microvilli), to 460.5 ± 35.8 and 601 ± 43.3 nM at 40–45 and 50–60 days in culture, respectively (n = 5 and 4; $P \leq 0.001$ vs. baseline). However, a flow-induced $[Ca^{2+}]_i$ response was not detected in tubules isolated from 21- to 25-day organoids (Fig. 2). Tubular cells in organoids cultured for 30–35 days exhibited a modest albeit significant increase in $[Ca^{2+}]_i$ in response to the onset of luminal flow.

The time interval between the onset of high luminal flow and peak $[Ca^{2+}]_i$ increased from 9.1 ± 1.3 s at 30–35 days, to 25.0 ± 0.5 s at 40–45 days, to 34.0 ± 2.2 s at 50–60 days (see Table 3 for number of cells and organoids). In tubules isolated from organoids cultured for >40 days, $[Ca^{2+}]_i$ decayed from the peak value to a modest plateau elevation in $[Ca^{2+}]_i$ that was sustained during the period of luminal flow (Fig. 2).

Basolateral Flow/FSS Increases $[Ca^{2+}]_i$ in Nonperfused Kidney Organoid Tubules

Nonperfused tubules isolated from H9 organoids cultured for 41 days and exposed to a 10-fold increase in superfusate (bath) flow rate from 10 to 100 mL/h exhibited a rapid increase in $[Ca^{2+}]_i$ from 212.3 ± 14.7 nM to 427.4 ± 98.1 nM (n = 31 cells in 8 organoids; $P < 0.001$ vs. baseline) before decaying to a plateau elevation (Fig. 3). The time interval between the increase in luminal flow and peak $[Ca^{2+}]_i$ was 7.5 ± 2.9 s. Pretreatment of tubules with GsMTx4, an inhibitor of mechanosensitive ion channels (48), completely suppressed the superfusate (bath)-triggered Ca^{2+} response (n = 22 cells in 4 organoids; Fig. 3).

PIEZO1 Protein and Transcript Are Expressed in Kidney Organoids

As Piezo1 channels are expressed along the basolateral membranes of differentiated distal tubules in the adult mouse kidney (34) and contribute to flow-induced $[Ca^{2+}]_i$ responses in these segments (49), we sought to examine whether PIEZO1 was expressed in maturing organoids. Immunodetectable PIEZO1 was expressed in multiple structures in maturing organoids (Fig. 4*A*). Although we were unable to precisely identify whether functional studies were performed in proximal or distal tubules, colabeling of organoids for PIEZO1 as well as LTL and CDH1, markers of proximal and distal tubules, respectively, revealed that only tubular structures, but not PODXL positive glomerular structures, expressed PIEZO1 (Fig. 4*B*). With advancing days in culture, the relative expression of immunodetectable PIEZO1 in organoid tubular cells appeared to diminish in the basolateral region and increase in the apical region (Fig. 4*C*). In addition, the density of apical cilia projecting into the lumen of the organoids, visualized using the marker acetylated α-tubulin (α-Ac-Tub), appeared to be more prominent with advancing age (Fig. 4*D*).

RNA-seq analyses of maturing organoids revealed a significant increase in *PIEZO1* transcript expression between *days 8* and *35* days in culture whereas *TRPV4* expression

Table 3. *Changes in $[Ca^{2+}]_i$ elicited by an increase in luminal flow rate*

Days in Culture	*N*, Organoids	*n*, Total Cells	Baseline $[Ca^{2+}]$, nM	Peak $[Ca^{2+}]$, nM	Time to Peak, s	Slope to Peak, nM/s
21–25	5	27	198.8 ± 11.7	205.7 ± 20.4		
30–35	4	30	187.6 ± 13.7	270.9 ± 35.6	9.1 ± 1.3	9.1 ± 1.1
40–45	5	35	190.4 ± 10.6	460.5 ± 25.8	25.0 ± 0.5*	11.1 ± 1.1*
50–60	4	26	201.0 ± 25.1	601.1 ± 43.3	34.0 ± 2.2*#	12.6 ± 3.2*

*$P \leq 0.001$ vs. 30–35 days and #$P \leq 0.001$ vs. 40.45 days.

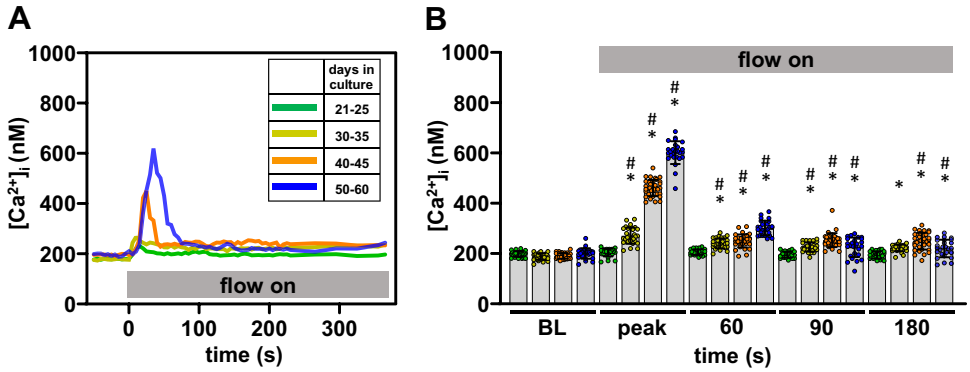

Figure 2. The luminal flow-induced $[Ca^{2+}]_i$ response is enhanced in microperfused tubules from kidney organoids (H9) cultured longitudinally. *A*: representative tracings of flow-induced changes in $[Ca^{2+}]_i$ in single tubules isolated from organoids at increasing days of culture. *B*: individual cell (circles) and mean (± SD) values of $[Ca^{2+}]_i$ are given at baseline (BL), flow-induced peak, and specific times during the period of sustained luminal flow. Tubules from organoids cultured for >30 days exhibited a peak $[Ca^{2+}]_i$ that significantly exceeded BL values. Tubules from organoids cultured for >40 days exhibited a modest plateau elevation in $[Ca^{2+}]_i$ during the period of sustained luminal flow. One tubule was assayed per organoid; see Table 3 for number of organoids and cells studied. The gray bar indicates the period of sustained high luminal flow. *$P \leq 0.001$ vs. BL and #$P \leq 0.001$ vs. 21–25 days by one-way multiple comparisons ANOVA (Holm–Sidak method).

levels remained stable throughout the period studied (Supplemental Fig. S1). Based on the results of the functional studies described above, we interrogated the RNAseq database to examine whether organoid maturation is accompanied by changes in expression of sarco/endoplasmic reticulum ATPase 3 (SERCA3), the major SERCA isoform detected in kidney (50), responsible for taking up Ca^{2+} from the cytosol into the ER, and the plasma membrane Ca^{2+} ATPase (PMCA1) and Na^+/Ca^{2+} exchanger (NCX1), proteins responsible for Ca^{2+} extrusion in renal epithelial cells (51–54). Both message and protein corresponding to these three proteins are expressed in human kidney as reported in the Human Protein Atlas (https://www.proteinatlas.org/). *PMCA1* expression increased significantly between *days 8* and *21* in culture (Supplemental Fig. S1). Transcript abundance of *SERCA3* and *NCX1* was low (Supplemental Fig. S1).

To validate the temporal changes in gene expression revealed by RNA-seq, we performed quantitative real-time PCR (qPCR) to measure expression levels of those genes with FPKM values >3. The qPCR results were concordant with the RNA-seq results for *PIEZO1* and *PMCA1* in terms of the trend of change in expression over time (Fig. 5). *TRPV4* expression levels at 49 days in culture exceeded that measured at *day 8*. Notably, we observed temporal changes in *ACTB* expression with advancing days in culture (Fig. 5), thus leading to the use of *GAPDH* as the reference gene for standardization of target gene expression.

Basolateral Piezo-Mediated $[Ca^{2+}]_i$ Response Is Enhanced in Microperfused Tubules Isolated from Kidney Organoids Cultured Longitudinally

To discern whether immunodetectable basolateral PIEZO1 was functional, we examined the effect on $[Ca^{2+}]_i$ in organoid tubules to the cell impermeant PIEZO1 agonist Yoda1. Yoda1 is known to induce a robust increase in $[Ca^{2+}]_i$ in HEK cells transfected with either human or mouse *Piezo1*, but not *Piezo2*, underscoring the selectivity of this agonist for Piezo1 (23). We first generated a dose-response curve to identify the optimal agonist concentration to use in these experiments

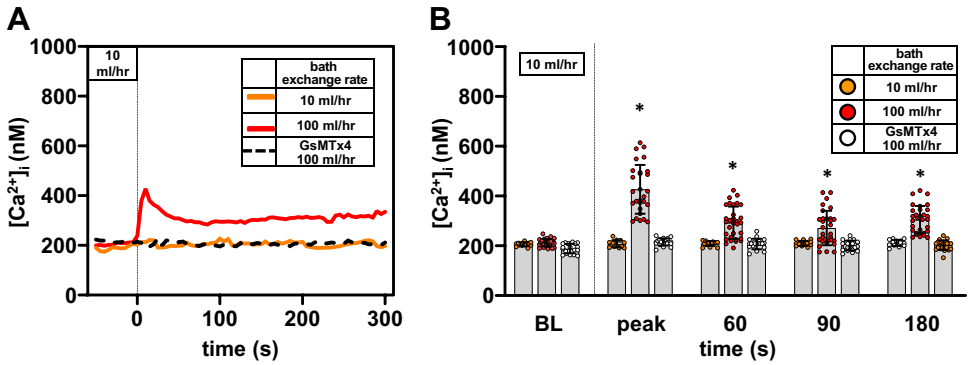

Figure 3. Basolateral flow/FSS increases $[Ca^{2+}]_i$ in nonperfused kidney organoid (H9) tubules. *A*: representative tracings of the effect of an increase in bath flow rate, in the absence of luminal flow, on $[Ca^{2+}]_i$ in single tubules isolated from organoids cultured for 41 days. *B*: individual cell (circles) and mean (± SD) values of $[Ca^{2+}]_i$ are given at baseline (BL), flow-induced peak, and specific times after a 10-fold increase in bath flow rate from 10 to 100 mL/h. At a slow bath fluid exchange rate, $[Ca^{2+}]_i$ remained stable, averaging ~200 nM. In response to an increase in bath flow rate, $[Ca^{2+}]_i$ increased rapidly before decaying to a plateau elevation during the period of sustained high flow. Bath flow rate was adjusted using a syringe pump. One tubule was assayed per organoid; 3 organoids were studied at each time point and 14–31 cells were analyzed in each group. *$P \leq 0.001$ vs. BL by one-way multiple comparisons ANOVA (Holm–Sidak method).

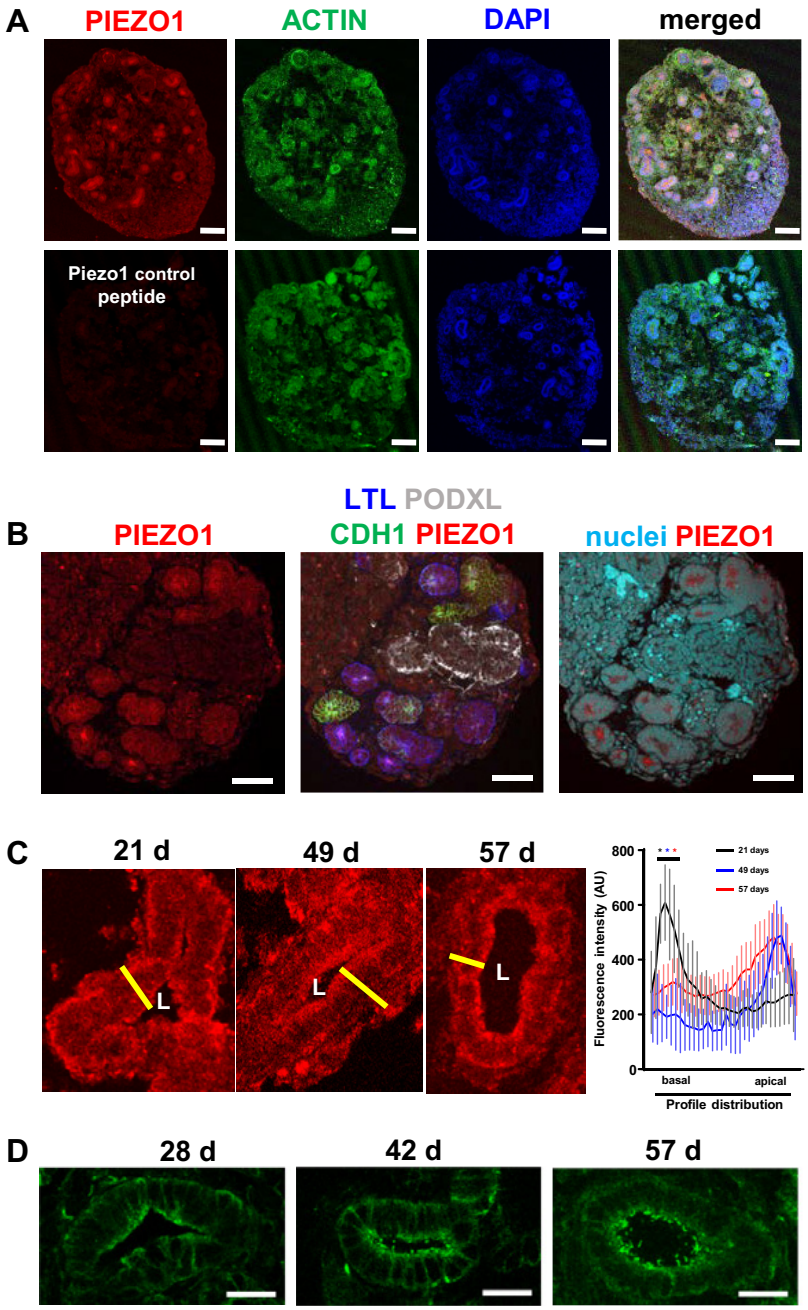

Figure 4. Subcellular PIEZO1 expression in maturing organoid tubules, visualized by confocal microscopy. *A*: immunodetectable PIEZO1 and actin are expressed in multiple structures in the organoid (49 days in culture), but PIEZO1 labeling is eliminated by preadsorption of the antibody with peptide. Bar = 100 μM. *B*: representative confocal micrographs of organoids labeled with antibodies directed against PIEZO1 (*left*) and structure/segment-specific markers (*middle*), demonstrating that both LTL-positive proximal tubules and CDH1-positive distal tubules express basolateral and apical PIEZO1 (*right*). Bar = 50 μM. *C*: representative images of cross sections of cryosections of organoids cultured for 21, 49, and 57 days showing PIEZO1 localization to both the apical and basolateral membranes of cells in tubular structures at all ages studied. The fluorescence signal corresponding to PIEZO1 along the line extending from the basolateral to apical membrane, in cells in profile, was calculated in at least 100 cells from 18–20 randomly chosen tubules in 4 organoids at each time point. The summary of these line scans is presented in the graph on the right. PIEZO1 distribution shifted toward the apical membrane in organoid tubular cells with advancing days in culture. L, lumen. AU, arbitrary units. At each of the 3 developmental stages examined, the peak values for basolateral and apical PIEZO1 expression were compared, with statistical differences determined by paired *t* test $*P < 0.001$. *D*: 3-D projections of 4 confocal stacks (steps of 1 μm) from cryostat sections of maturing organoids immunolabeled with anti-acetylated α-tubulin, which labels cilia. The density of apical cilia appeared more prominent with increasing days in culture. Bar = 20 μm.

(Fig. 6, *A* and *B*). Yoda1 concentrations as high as 10 μM added in the bath did not appear to be toxic to the organoid tubules, evidenced by trypan blue exclusion from these structures (Fig. 6*C*). Although basolateral 1 μM Yoda1 elicited a modest increase in the fura-2 FIR, reflecting $[Ca^{2+}]_i$, a concentration of ~5 μM generated a maximal $[Ca^{2+}]_i$ response (Fig. 6*A*), leading us to use this concentration for subsequent studies.

Addition of 5 μM Yoda1 to the solution bathing nonperfused tubules isolated from H9 (Figs. 7, *A* and *B*) and BJFF (Figs. 7, *C* and *D*) organoids cultured for >30 days led to a gradual increase in $[Ca^{2+}]_i$ above baseline, consistent with the presence of functional basolateral PIEZO1 channels. The magnitude of the Yoda1-induced $[Ca^{2+}]_i$ response increased with increasing days in culture, consistent with a maturational increase in number and/or activity of PIEZO1 channels. Yoda1 had no effect on $[Ca^{2+}]_i$ in tubules isolated from 22- to 25-day organoids.

DISCUSSION

Glomerular and tubular structures within organoids cultured in vitro while continuously exposed to a sustained mechanical stress arising from superfusate (bath) flow exhibited enhanced morphological maturation (10). As FSS, CS and/or drag/torque on cilia/microvilli lead to $[Ca^{2+}]_i$ transients in renal epithelial cells in the fully differentiated kidney (11) and Ca^{2+} signaling contributes to key pattern forming events (37, 55, 56), we sought to examine whether organoid tubular structures respond to luminal and/or basolateral (superfusate) flow

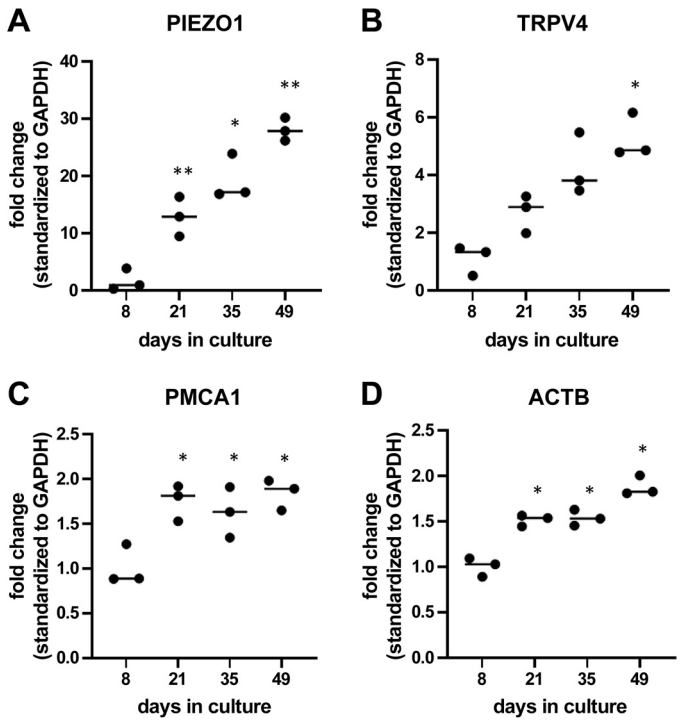

Figure 5. RT-qPCR of genes encoding Ca^{2+} transport proteins *PIEZO1* (*A*), *TRPV4* (*B*), and *PMCA1* (*C*) in kidney organoids over time, standardized to *GAPDH* expression levels and normalized to expression at *day 8*. *D*: RT-qPCR of *ACTB* (encoding β-actin), also standardized to *GAPDH* expression, in kidney organoids over time. Dot plots show means for individual organoids at the given days in culture. Data represent the mean of 3 organoids for all days. Statistical significance was determined by paired Tukey's *t* tests with $*P < 0.05$ and $**P < 0.01$ vs. *day 8*.

with an increase in $[Ca^{2+}]_i$ and identify the proximate mechanosensor in this pathway. Specifically, we aimed to examine the role of the mechanosensitive PIEZO1 Ca^{2+} channel in organoid maturation given that this protein is *1*) required for vascular development and cell rearrangements in response to flow (28–31), *2*) gated in part by direct membrane tension (57, 58), and *3*) present in the basolateral membrane of fully differentiated mouse distal nephron tubules (34), an ideal location to sense an increase in membrane tension induced by an increase in tubule diameter and/or basolateral mechanical perturbation. Indeed, our laboratory has previously reported that Piezo1 mediates an increase in $[Ca^{2+}]_i$ in response to an increase in luminal flow rate in the fully differentiated rodent renal collecting duct (49).

The results of the present study show that an increase in luminal flow rate, likely triggering apical FSS, CS, and/or drag/torque on cilia/microvilli, increases $[Ca^{2+}]_i$ in epithelial cells lining tubular structures in organoids cultured for at least 30 days and the magnitude of the increase in $[Ca^{2+}]_i$ increases with days in culture (Fig. 2). Consistent with our previous observation that the luminal flow-induced $[Ca^{2+}]_i$ response in fully differentiated tubules reflects not only luminal but also basolateral Ca^{2+} entry (11), we now demonstrate that an increase in bath flow rate in the absence of luminal flow also leads to an increase in $[Ca^{2+}]_i$ in nonperfused organoid tubules (Fig. 3). The sensitivity of this response to the mechanosensitive ion channel inhibitor GsMTx4 suggests that mechanoinduced basolateral Ca^{2+} entry is mediated by mechanosensitive ion channels.

We posited that the molecular identity of this basolateral Ca^{2+} entry pathway is the PIEZO1 channel which is supported by our observation that basolateral Yoda1, a PIEZO1 agonist, increased $[Ca^{2+}]_i$ in an age-dependent manner in nonperfused segments (Fig. 7), consistent with a developmental increase in number and/or activity of basolateral PIEZO1 channels. Although we did not quantitate total PIEZO1 protein expression in maturing organoids (Fig. 4), the increase in *PIEZO1* transcript abundance in kidney organoids detected between *days 8* and *49* of culture/differentiation (Fig. 5) suggests it likely that basolateral PIEZO1 abundance increases in organoid tubules with advancing days in culture. The delay between appearance of immunodetectable PIEZO1 in 21-day organoids and functional responsiveness to Yoda1 by 30 days may reflect low levels of PIEZO1 protein expression in organoids cultured for <30 days, as suggested by the lower abundance of *PIEZO1* transcript detected in these young organoids (Fig. 5). Note that studies in artificial lipid bilayers have shown that activation of PIEZO1 by Yoda1 does not require

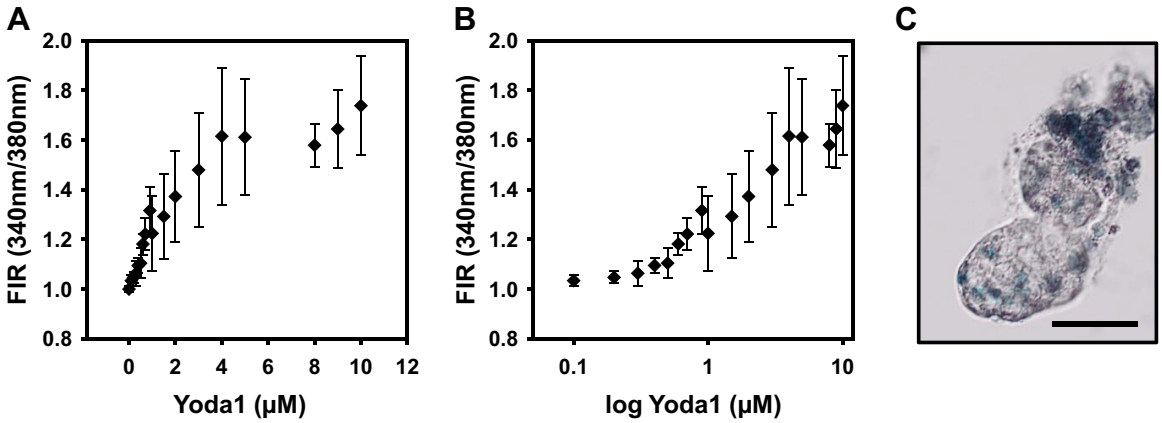

Figure 6. Effect of Yoda1 on $[Ca^{2+}]_i$ in tubules isolated from static organoids (H9) cultured for 22–27 days. *A* and *B*: dose-response (fluorescence intensity ratio, FIR) curves for Yoda1 added to the solution bathing fura-2-loaded organoids. A bath concentration of 4 μM Yoda1 generated a maximal increase in FIR. *n* = 20 cells in 4 tubules. One tubule was studied per organoid. *C*: 10 min after exposure to 10 μM Yoda1, trypan blue was excluded from tubular structures but was taken up into cells adherent to the tubular structures. Bar = 40 μm.

AJP-Cell Physiol • doi:10.1152/ajpcell.00288.2022 • www.ajpcell.org

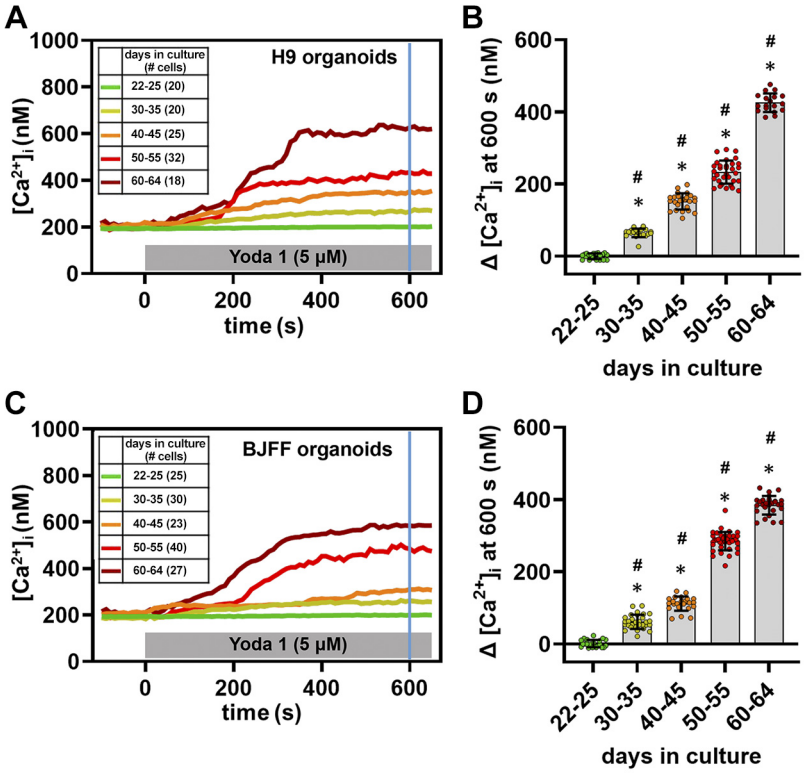

Figure 7. Basolateral PIEZO1-mediated $[Ca^{2+}]_i$ response is enhanced in tubules from kidney organoids cultured longitudinally. *A* and *C*: representative tracings of basolateral 5 μM Yoda1-induced changes in $[Ca^{2+}]_i$ in tubules isolated from H9 (*top*) and BJFF (*bottom*) organoids at increasing days in culture. The number of cells studied is indicated parentheses. *B* and *D*: individual cell (circles) and mean (± SD) values of the change (Δ) in $[Ca^{2+}]_i$ from baseline measured at steady state (600 s) after addition of Yoda1 to the solution bathing tubules isolated from H9 (*top*) and BJFF (*bottom*) organoids. All tubules isolated from organoids cultured for >25 days exhibited a Yoda1-induced increase in $[Ca^{2+}]_i$ above baseline, consistent with the presence of basolateral PIEZO1 channels. The $[Ca^{2+}]_i$ response of organoid tubules to bath Yoda1 increased with increasing days in culture, consistent with a maturational increase in number and/or activity of PIEZO1 channels. 18–40 cells in 4–6 organoids were studied at each age; 1 tubule was assayed per organoid. $*P \leq 0.001$ vs. time 0 (before exposure to Yoda1) by two-tailed *t* test. $\#P \leq 0.001$ vs. 22–25 days by one-way multiple comparisons ANOVA (Holm–Sidak method).

other cellular components (23), such as signaling pathways that might be developmentally regulated.

The time interval between onset of luminal flow and peak $[Ca^{2+}]_i$ response in microperfused organoid tubules increased from 9 s at 30–35 days to 34 s at 50–60 days in culture (Fig. 2, Table 3). Praetorius and Spring (59) reported that direct mechanical stimulation of the apical membrane of monolayers of MDCK cells led to a maximal 1.9-fold increase in $[Ca^{2+}]_i$ within 10 s whereas the time interval to the 1.6-fold increase in $[Ca^{2+}]_i$ triggered by direct bending of the apical cilium was ~36 s. The authors further found that the $[Ca^{2+}]_i$ response elicited by application of mechanical forces directly to the cell membrane was independent of extracellular Ca^{2+} whereas that generated by cilia bending was dependent on extracellular Ca^{2+} entry through stretch-activated nonselective cation channels (59). Based on these studies, we speculate that the time delay to peak response elicited by flow with advancing days in culture likely reflects the maturation of flow sensor(s) and signal transduction pathways mediating this response. In fact, organoid tubules cultured for <35 days were characterized by an apparent paucity of apical cilia (Fig. 4) suggesting it likely that their rapid time (<10 s) to luminal flow-induced peak $[Ca^{2+}]_i$ (Table 3) was due to mechanical perturbation of the apical membrane. By *day 56* of culture, organoid tubules appeared to possess a high density of apical cilia (Fig. 4). In these more mature tubules, the increase in luminal flow is likely to have induced bending of the apical cilia and, based on the studies of Praetorius and Spring (59), would be expected to lead to a relatively delayed time to maximal $[Ca^{2+}]_i$ response, as observed (Fig. 2, Table 3). The contribution of the relative increase in immunodetectable apical versus basolateral PIEZO1 expression in more mature organoid tubules (Fig. 4*C*) to their luminal flow-induced Ca^{2+} response has yet to be evaluated.

We observed that tubules from organoids cultured for >40 days exhibited a modest plateau elevation in $[Ca^{2+}]_i$ during a period of sustained luminal flow. We have previously reported that in the adult rodent, this plateau elevation in $[Ca^{2+}]_i$, reflects luminal Ca^{2+} entry that is, in part, mediated by TRPV4 (13–17). Our detection of a significant increase in *TRPV4* expression only after 35 days in culture (Fig. 5) predicts it likely that tubules isolated from organoids cultured for less than 35 days should not exhibit a plateau elevation in $[Ca^{2+}]_i$ in response to luminal flow. As the focus of this study was on PIEZO1, we did not evaluate whether TRPV4 protein was present or functional in differentiating organoids.

We noted that the resting $[Ca^{2+}]_i$ in organoid tubules averaged ~195 nM at all stages studied, a concentration that is almost double that measured in fully differentiated rodent distal nephron epithelial cells (11, 18, 40, 41, 49). However, measurements of $[Ca^{2+}]_i$ in fura-2-loaded rodent proximal tubules range from ~150–200 nM (60–62). To our knowledge, our absolute $[Ca^{2+}]_i$ measurements in organoid epithelial structures are the first to be reported; a review of the literature reveals that most other investigators who have studied organoids used nonratiometric single wavelength probes (Fluo-4) that can report changes in signal intensity from baseline but not absolute concentrations, or if using fura-2, reported only FIRs.

$[Ca^{2+}]_i$ is tightly regulated by the activity of Ca^{2+} pumps and exchangers in the plasma membrane and the balance of Ca^{2+} release and uptake from intracellular stores, for example, the endoplasmic reticulum (ER). We have previously reported that the mechanoinduced increase in $[Ca^{2+}]_i$ in

rodent distal nephron reflects both the release of Ca^{2+} from inositol triphosphate (IP3)-sensitive intracellular stores and influx of Ca^{2+} from the extracellular space across the plasma membrane (11). Specifically, we proposed that the luminal flow-induced initial rapid increase in $[Ca^{2+}]_i$ to a peak value in the distal nephron reflects basolateral Ca^{2+} influx coupled to Ca^{2+} release from ER stores (Calcium-Induced Calcium Release, or CICR) and that depletion of ER stores triggers Store Operated Calcium Entry (SOCE) across the plasma membrane causing opening of plasma membrane Ca^{2+} channels to promote refilling of the ER stores (11, 63). In response to an increase in $[Ca^{2+}]_i$, Ca^{2+} is extruded from renal epithelial cells to the extracellular space by the plasma membrane Ca^{2+} ATPase (PMCA) and the Na^+/Ca^{2+} exchanger (NCX) (64). It is also worth noting that matrix stiffness has been shown to influence $[Ca^{2+}]_i$ signaling in cancer cell cultures (65).

Based on the signaling pathways summarized above, we speculated that the slower time to peak $[Ca^{2+}]_i$ in younger organoids might reflect lower rates of Ca^{2+} entry into the cells due to low abundance of PIEZO1 and/or TRPV4. Indeed, transcript expression for these two Ca^{2+} entry pathways, assessed by qPCR, increased significantly between 8 and 49 days of culture. Furthermore, we considered that the higher baseline $[Ca^{2+}]_i$ in organoids compared with that measured in the adult rodent is due in part to low expression of proteins responsible for Ca^{2+} extrusion, including PMCA1 and NCX1. Although *NCX1* transcript expression was low in all organoids studied, *PMCA1* transcript expression increased significantly between *days 8* and *21* of culture, then remaining relatively stable (by qPCR) or falling slightly (by qPCR) by *day 49*. In sum, these data suggest that Ca^{2+} entry and extrusion pathways in kidney organoids are regulated with advancing days in culture. Given that the reliability of RT-qPCR data depends on the stable expression levels of reference genes among cells in different tissues, our observation of a developmental change in abundance of *ACTB* over time underscores the need for a future study to identify the most appropriate reference gene(s) for normalization of qPCR data in maturing organoids.

Identification of a maturational increase in functional PIEZO1 activity at the basolateral membrane of organoid tubules in culture begs the question as to its function during differentiation. Studies are ongoing to determine whether PIEZO1 activation by addition of Yoda1 to the solution bathing organoids cultured under static conditions can reproduce the effect of superfusate (bath) flow in stimulating morphologic and functional maturation of organoids. Indeed, Yoda1 (up to 2 μM) added to static cultures of endothelial cells has been reported to mimic the effects of FSS on phenotypic differentiation, specifically expression of cell adhesion molecules (66). Precise delineation of the "time window" during which active PIEZO1 channels first appear in maturing kidney organoids is clearly a necessary first step in designing future experiments to discern whether this mechanosensitive channel contributes to organoid differentiation.

DATA AVAILABILITY

Data will be made available upon reasonable request.

SUPPLEMENTAL DATA

Supplemental Fig. S1: https://doi.org/10.6084/m9.figshare.21950621.v1.

ACKNOWLEDGMENTS

Immunofluorescence confocal microscopy at the ISMMS was performed in the Microscopy CoRE. We acknowledge the technical help of Joanne Soong at the ISMMS, Kazumi Ida at Massachusetts General Hospital, and Mariana Mata at Harvard University.

GRANTS

This work was supported by grants from the National Institutes of Health, including the (Re)Building A Kidney Consortium UC2DK126023 (to J.A.L., L.S., and R.M.), DP2 DK133821 (to R.M.), R01 DK038470 (to L.M.S.), R01 DK129285 (to L.M.S.), and P30 DK079307 (to L.M.S.).

DISCLOSURES

J.A.L. and R.M. are coinventors on patents (PCT/US2018/036677) that are assigned to President and Fellows of Harvard College and Mass General Brigham. J.A.L. and R.M. serve on the Scientific Advisory Board of Trestle Biotherapeutics, which has licensed technology from their labs. None of the other authors has any conflicts of interest, financial or otherwise, to disclose.

AUTHOR CONTRIBUTIONS

R.C-G., K.T.K., K.H., R.M., J.A.L., and L.M.S. conceived and designed research; R.C-G., K.H., R.M., and L.M.S. performed experiments; R.C-G., K.H., N.R.G., R.M., and L.M.S. analyzed data; R.C-G., K.T.K., K.H., N.R.G., R.M., J.A.L., and L.M.S. interpreted results of experiments; R.C-G., R.M., and L.M.S. prepared figures; R.C-G., R.M., and L.M.S. drafted manuscript; R.C-G., K.T.K., K.H., R.M., J.A.L., and L.M.S. edited and revised manuscript; R.C-G., K.T.K., K.H., N.R.G., R.M., J.A.L., and L.M.S. approved final version of manuscript.

REFERENCES

1. **Chanet S**, **Martin AC.** Mechanical force sensing in tissues. *Prog Mol Biol Transl Sci* 126: 317–352, 2014. doi:10.1016/B978-0-12-394624-9.00013-0.
2. **Daems M**, **Peacock HM**, **Jones EAV.** Fluid flow as a driver of embryonic morphogenesis. *Development* 147: dev185579, 2020. doi:10.1242/dev.185579.
3. **Hannezo E**, **Heisenberg CP.** Mechanochemical feedback loops in development and disease. *Cell* 178: 12–25, 2019. doi:10.1016/j.cell.2019.05.052.
4. **Heisenberg CP**, **Bellaïche Y.** Forces in tissue morphogenesis and patterning. *Cell* 153: 948–962, 2013. doi:10.1016/j.cell.2013.05.008.
5. **Kim S**, **Uroz M**, **Bays JL**, **Chen CS.** Harnessing mechanobiology for tissue engineering. *Dev Cell* 56: 180–191, 2021. doi:10.1016/j.devcel.2020.12.017.
6. **Vining KH**, **Mooney DJ.** Mechanical forces direct stem cell behaviour in development and regeneration. *Nat Rev Mol Cell Biol* 18: 728–742, 2017. doi:10.1038/nrm.2017.108.
7. **Takasato M**, **Er PX**, **Chiu HS**, **Maier B**, **Baillie GJ**, **Ferguson C**, **Parton RG**, **Wolvetang EJ**, **Roost MS**, **Chuva de Sousa Lopes SM**, **Little MH.** Kidney organoids from human iPS cells contain multiple lineages and model human nephrogenesis. *Nature* 526: 564–568, 2015. doi:10.1038/nature15695.
8. **van den Berg CW**, **Ritsma L**, **Avramut MC**, **Wiersma LE**, **van den Berg BM**, **Leuning DG**, **Lievers E**, **Koning M**, **Vanslambrouck JM**, **Koster AJ**, **Howden SE**, **Takasato M**, **Little MH**, **Rabelink TJ.** Renal

subcapsular transplantation of PSC-derived kidney organoids induces neo-vasculogenesis and significant glomerular and tubular maturation in vivo. *Stem Cell Reports* 10: 751–765, 2018. doi:10.1016/j.stemcr.2018.01.041.

9. **Wu H**, **Uchimura K**, **Donnelly EL**, **Kirita Y**, **Morris SA**, **Humphreys BD.** Comparative analysis and refinement of human PSC-derived kidney organoid differentiation with single-cell transcriptomics. *Cell Stem Cell* 23: 869–881.e8, 2018. doi:10.1016/j.stem.2018.10.010.
10. **Homan KA**, **Gupta N**, **Kroll KT**, **Kolesky DB**, **Skylar-Scott M**, **Miyoshi T**, **Mau D**, **Valerius MT**, **Ferrante T**, **Bonventre JV**, **Lewis JA**, **Morizane R.** Flow-enhanced vascularization and maturation of kidney organoids in vitro. *Nat Methods* 16: 255–262, 2019. doi:10.1038/s41592-019-0325-y.
11. **Liu W**, **Xu S**, **Woda C**, **Kim P**, **Weinbaum S**, **Satlin LM.** Effect of flow and stretch on the [Ca^{2+}]i response of principal and intercalated cells in cortical collecting duct. *Am J Physiol Renal Physiol* 285: F998–F1012, 2003. doi:10.1152/ajprenal.00067.2003.
12. **Carrisoza-Gaytan R**, **Carattino MD**, **Kleyman TR**, **Satlin LM.** An unexpected journey: conceptual evolution of mechanoregulated potassium transport in the distal nephron. *Am J Physiol Cell Physiol* 310: C243–C259, 2016. doi:10.1152/ajpcell.00328.2015.
13. **Li Y**, **Hu H**, **Butterworth MB**, **Tian JB**, **Zhu MX**, **O'Neil RG.** Expression of a diverse array of Ca^{2+}-activated K^+ channels (SK1/3, IK1, BK) that functionally couple to the mechanosensitive TRPV4 channel in the collecting duct system of kidney. *PLoS One* 11: e0155006, 2016. doi:10.1371/journal.pone.0155006.
14. **Berrout J**, **Jin M**, **Mamenko M**, **Zaika O**, **Pochynyuk O**, **O'Neil RG.** Function of transient receptor potential cation channel subfamily V member 4 (TRPV4) as a mechanical transducer in flow-sensitive segments of renal collecting duct system. *J Biol Chem* 287: 8782–8791, 2012. doi:10.1074/jbc.M111.308411.
15. **Taniguchi J**, **Tsuruoka S**, **Mizuno A**, **Sato J**, **Fujimura A**, **Suzuki M.** TRPV4 as a flow sensor in flow-dependent K+ secretion from the cortical collecting duct. *Am J Physiol Renal Physiol* 292: F667–F673, 2007. doi:10.1152/ajprenal.00458.2005.
16. **Pochynyuk O**, **Zaika O**, **O'Neil RG**, **Mamenko M.** Novel insights into TRPV4 function in the kidney. *Pflugers Arch* 465: 177–186, 2013. doi:10.1007/s00424-012-1190-z.
17. **Liu W**, **Morimoto T**, **Woda C**, **Kleyman TR**, **Satlin LM.** Ca^{2+} dependence of flow-stimulated K secretion in the mammalian cortical collecting duct. *Am J Physiol Renal Physiol* 293: F227–F235, 2007. doi:10.1152/ajprenal.00057.2007.
18. **Liu W**, **Murcia NS**, **Duan Y**, **Weinbaum S**, **Yoder BK**, **Schwiebert E**, **Satlin LM.** Mechanoregulation of intracellular Ca^{2+} concentration is attenuated in collecting duct of monocilium-impaired orpk mice. *Am J Physiol Renal Physiol* 289: F978–F988, 2005. doi:10.1152/ajprenal.00260.2004.
19. **Woda CB**, **Miyawaki N**, **Ramalakshmi S**, **Ramkumar M**, **Rojas R**, **Zavilowitz B**, **Kleyman TR**, **Satlin LM.** Ontogeny of flow-stimulated potassium secretion in rabbit cortical collecting duct: functional and molecular aspects. *Am J Physiol Renal Physiol* 285: F629–F639, 2003. doi:10.1152/ajprenal.00191.2003.
20. **Coste B**, **Mathur J**, **Schmidt M**, **Earley TJ**, **Ranade S**, **Petrus MJ**, **Dubin AE**, **Patapoutian A.** Piezo1 and Piezo2 are essential components of distinct mechanically activated cation channels. *Science* 330: 55–60, 2010. doi:10.1126/science.1193270.
21. **Coste B**, **Xiao B**, **Santos JS**, **Syeda R**, **Grandl J**, **Spencer KS**, **Kim SE**, **Schmidt M**, **Mathur J**, **Dubin AE**, **Montal M**, **Patapoutian A.** Piezo proteins are pore-forming subunits of mechanically activated channels. *Nature* 483: 176–181, 2012. doi:10.1038/nature10812.
22. **Volkers L**, **Mechioukhi Y**, **Coste B.** Piezo channels: from structure to function. *Pflugers Arch* 467: 95–99, 2015. doi:10.1007/s00424-014-1578-z.
23. **Syeda R**, **Xu J**, **Dubin AE**, **Coste B**, **Mathur J**, **Huynh T**, **Matzen J**, **Lao J**, **Tully DC**, **Engels IH**, **Petrassi HM**, **Schumacher AM**, **Montal M**, **Bandell M**, **Patapoutian A.** Chemical activation of the mechanotransduction channel Piezo1. *eLife* 4: e07369, 2015. doi:10.7554/eLife.07369.
24. **Gottlieb PA**, **Sachs F.** Piezo1: properties of a cation selective mechanical channel. *Channels (Austin)* 6: 214–219, 2012. doi:10.4161/chan.21050.
25. **Syeda R**, **Florendo MN**, **Cox CD**, **Kefauver JM**, **Santos JS**, **Martinac B**, **Patapoutian A.** Piezo1 channels are inherently mechanosensitive. *Cell Rep* 17: 1739–1746, 2016. doi:10.1016/j.celrep.2016.10.033.
26. **Peyronnet R**, **Martins JR**, **Duprat F**, **Demolombe S**, **Arhatte M**, **Jodar M**, **Tauc M**, **Duranton C**, **Paulais M**, **Teulon J**, **Honoré E**, **Patel A.** Piezo1-dependent stretch-activated channels are inhibited by Polycystin-2 in renal tubular epithelial cells. *EMBO Rep* 14: 1143–1148, 2013. doi:10.1038/embor.2013.170.
27. **Miyamoto T**, **Mochizuki T**, **Nakagomi H**, **Kira S**, **Watanabe M**, **Takayama Y**, **Suzuki Y**, **Koizumi S**, **Takeda M**, **Tominaga M.** Functional role for Piezo1 in stretch-evoked Ca^{2+} influx and ATP release in urothelial cell cultures. *J Biol Chem* 289: 16565–16575, 2014. doi:10.1074/jbc.M113.528638.
28. **Kang H**, **Hong Z**, **Zhong M**, **Klomp J**, **Bayless KJ**, **Mehta D**, **Karginov AV**, **Hu G**, **Malik AB.** Piezo1 mediates angiogenesis through activation of MT1-MMP signaling. *Am J Physiol Cell Physiol* 316: C92–C103, 2019. doi:10.1152/ajpcell.00346.2018.
29. **Ranade SS**, **Qiu Z**, **Woo SH**, **Hur SS**, **Murthy SE**, **Cahalan SM**, **Xu J**, **Mathur J**, **Bandell M**, **Coste B**, **Li YS**, **Chien S**, **Patapoutian A.** Piezo1, a mechanically activated ion channel, is required for vascular development in mice. *Proc Natl Acad Sci USA* 111: 10347–10352, 2014. doi:10.1073/pnas.1409233111.
30. **Li J**, **Hou B**, **Tumova S**, **Muraki K**, **Bruns A**, **Ludlow MJ**, **Sedo A**, **Hyman AJ**, **McKeown L**, **Young RS**, **Yuldasheva NY**, **Majeed Y**, **Wilson LA**, **Rode B**, **Bailey MA**, **Kim HR**, **Fu Z**, **Carter DA**, **Bilton J**, **Imrie H**, **Ajuh P**, **Dear TN**, **Cubbon RM**, **Kearney MT**, **Prasad RK**, **Evans PC**, **Ainscough JF**, **Beech DJ.** Piezo1 integration of vascular architecture with physiological force. *Nature* 515: 279–282, 2014. doi:10.1038/nature13701.
31. **Eisenhoffer GT**, **Loftus PD**, **Yoshigi M**, **Otsuna H**, **Chien CB**, **Morcos PA**, **Rosenblatt J.** Crowding induces live cell extrusion to maintain homeostatic cell numbers in epithelia. *Nature* 484: 546–549, 2012. doi:10.1038/nature10999.
32. **Woo SH**, **Ranade S**, **Weyer AD**, **Dubin AE**, **Baba Y**, **Qiu Z**, **Petrus M**, **Miyamoto T**, **Reddy K**, **Lumpkin EA**, **Stucky CL**, **Patapoutian A.** Piezo2 is required for Merkel-cell mechanotransduction. *Nature* 509: 622–626, 2014. doi:10.1038/nature13251.
33. **He L**, **Si G**, **Huang J**, **Samuel ADT**, **Perrimon N.** Mechanical regulation of stem-cell differentiation by the stretch-activated Piezo channel. *Nature* 555: 103–106, 2018. doi:10.1038/nature25744.
34. **Dalghi MG**, **Clayton DR**, **Ruiz WG**, **Al-Bataineh MM**, **Satlin LM**, **Kleyman TR**, **Ricke WA**, **Carattino MD**, **Apodaca G.** Expression and distribution of PIEZO1 in the mouse urinary tract. *Am J Physiol Renal Physiol* 317: F303–F321, 2019. doi:10.1152/ajprenal.00214.2019.
35. **Jaffe LF.** Organization of early development by calcium patterns. *Bioessays* 21: 657–667, 1999. doi:10.1002/(SICI)1521-1878(199908)21:8<657::AID-BIES5>3.0.CO;2-K.
36. **Berridge MJ**, **Lipp P**, **Bootman MD.** The versatility and universality of calcium signalling. *Nat Rev Mol Cell Biol* 1: 11–21, 2000. doi:10.1038/35036035.
37. **Webb SE**, **Miller AL.** Calcium signalling during embryonic development. *Nat Rev Mol Cell Biol* 4: 539–551, 2003. doi:10.1038/nrm1149.
38. **Morizane R**, **Bonventre JV.** Generation of nephron progenitor cells and kidney organoids from human pluripotent stem cells. *Nat Protoc* 12: 195–207, 2017. doi:10.1038/nprot.2016.170.
39. **Morizane R**, **Lam AQ**, **Freedman BS**, **Kishi S**, **Valerius MT**, **Bonventre JV.** Nephron organoids derived from human pluripotent stem cells model kidney development and injury. *Nat Biotechnol* 33: 1193–1200, 2015. doi:10.1038/nbt.3392.
40. **Carrisoza-Gaytan R**, **Ray EC**, **Flores D**, **Marciszyn AL**, **Wu P**, **Liu L**, **Subramanya AR**, **Wang W**, **Sheng S**, **Nkashama LJ**, **Chen J**, **Jackson EK**, **Mutchler SM**, **Heja S**, **Kohan DE**, **Satlin LM**, **Kleyman TR.** Intercalated cell BKα subunit is required for flow-induced K^+ secretion. *JCI Insight* 5: e130553, 2020. doi:10.1172/jci.insight.130553.
41. **Carrisoza-Gaytán R**, **Wang L**, **Schreck C**, **Kleyman TR**, **Wang WH**, **Satlin LM.** The mechanosensitive BKα/β1 channel localizes to cilia of principal cells in rabbit cortical collecting duct (CCD). *Am J Physiol Renal Physiol* 312: F143–F156, 2017. doi:10.1152/ajprenal.00256.2016.
42. **Wang Y**, **Chi S**, **Guo H**, **Li G**, **Wang L**, **Zhao Q**, **Rao Y**, **Zu L**, **He W**, **Xiao B.** A lever-like transduction pathway for long-distance chemical- and mechano-gating of the mechanosensitive Piezo1 channel. *Nat Commun* 9: 1300, 2018. doi:10.1038/s41467-018-03570-9.
43. **Bae C**, **Sachs F**, **Gottlieb PA.** The mechanosensitive ion channel Piezo1 is inhibited by the peptide GsMTx4. *Biochemistry* 50: 6295–6300, 2011. doi:10.1021/bi200770q.

44. **Gnanasambandam R**, **Ghatak C**, **Yasmann A**, **Nishizawa K**, **Sachs F**, **Ladokhin AS**, **Sukharev SI**, **Suchyna TM.** GsMTx4: mechanism of inhibiting mechanosensitive ion channels. *Biophys J* 112: 31–45, 2017. doi:10.1016/j.bpj.2016.11.013.
45. **Grynkiewicz G**, **Poenie M**, **Tsien RY.** A new generation of Ca^{2+} indicators with greatly improved fluorescence properties. *J Biol Chem* 260: 3440–3450, 1985.
46. **Gupta N**, **Matsumoto T**, **Hiratsuka K**, **Garcia Saiz E**, **Galichon P**, **Miyoshi T**, **Susa K**, **Tatsumoto N**, **Yamashita M**, **Morizane R.** Modeling injury and repair in kidney organoids reveals that homologous recombination governs tubular intrinsic repair. *Sci Transl Med* 14: eabj4772, 2022 [Erratum in *Sci Transl Med* 14: eadd0524, 2022]. doi:10.1126/scitranslmed.abj4772.
47. **Valencia L**, **Melendez E**, **Namorado MC**, **Martin D**, **Bidet M**, **Poujeol P**, **Reyes JL.** Parathyroid hormone increases cytosolic calcium in neonatal nephron through protein kinase C pathway. *Pediatr Nephrol* 19: 1093–1101, 2004. doi:10.1007/s00467-004-1542-9.
48. **Bowman CL**, **Gottlieb PA**, **Suchyna TM**, **Murphy YK**, **Sachs F.** Mechanosensitive ion channels and the peptide inhibitor GsMTx-4: history, properties, mechanisms and pharmacology. *Toxicon* 49: 249–270, 2007. doi:10.1016/j.toxicon.2006.09.030.
49. **Carrisoza-Gaytan R**, **Dalghi MG**, **Apodaca GL**, **Kleyman TR**, **Satlin LM.** Piezo1 channels contribute to flow-induced intracellular calcium transients in mouse cortical collecting duct (CCD). *FASEB J* 33: 824.25, 2019. doi:10.1096/fasebj.2019.33.1_supplement.824.25.
50. **Martin V**, **Bredoux R**, **Corvazier E**, **Van Gorp R**, **Kovacs T**, **Gelebart P**, **Enouf J.** Three novel sarco/endoplasmic reticulum Ca^{2+}-ATPase (SERCA) 3 isoforms. Expression, regulation, and function of the membranes of the SERCA3 family. *J Biol Chem* 277: 24442–24452, 2002. doi:10.1074/jbc.M202011200.
51. **Carafoli E**, **Krebs J.** Why calcium? How calcium became the best communicator. *J Biol Chem* 291: 20849–20857, 2016. doi:10.1074/jbc.R116.735894.
52. **Stauffer TP**, **Guerini D**, **Carafoli E.** Tissue distribution of the four gene products of the plasma membrane Ca2+ pump. A study using specific antibodies. *J Biol Chem* 270: 12184–12190, 1995. doi:10.1074/jbc.270.20.12184.
53. **Lytton J.** Na^{+}/Ca^{2+} exchangers: three mammalian gene families control Ca^{2+} transport. *Biochem J* 406: 365–382, 2007. doi:10.1042/BJ20070619.
54. **van Loon EP**, **Little R**, **Prehar S**, **Bindels RJ**, **Cartwright EJ**, **Hoenderop JG.** Calcium extrusion pump PMCA4: a new player in renal calcium handling? *PLoS One* 11: e0153483, 2016. doi:10.1371/journal.pone.0153483.
55. **Brodskiy PA**, **Zartman JJ.** Calcium as a signal integrator in developing epithelial tissues. *Phys Biol* 15: 051001, 2018. doi:10.1088/1478-3975/aabb18.
56. **Berridge MJ**, **Bootman MD**, **Roderick HL.** Calcium signalling: dynamics, homeostasis and remodelling. *Nat Rev Mol Cell Biol* 4: 517–529, 2003. doi:10.1038/nrm1155.
57. **Murthy SE**, **Dubin AE**, **Patapoutian A.** Piezos thrive under pressure: mechanically activated ion channels in health and disease. *Nat Rev Mol Cell Biol* 18: 771–783, 2017. doi:10.1038/nrm.2017.92.
58. **Cox CD**, **Bavi N**, **Martinac B.** Origin of the force: the force-from-lipids principle applied to Piezo channels. *Curr Top Membr* 79: 59–96, 2017. doi:10.1016/bs.ctm.2016.09.001.
59. **Praetorius HA**, **Spring KR.** Bending the MDCK cell primary cilium increases intracellular calcium. *J Membr Biol* 184: 71–79, 2001. doi:10.1007/s00232-001-0075-4.
60. **Yamada H**, **Seki G**, **Taniguchi S**, **Uwatoko S**, **Suzuki K**, **Kurokawa K.** Mechanism of $[Ca^{2+}]i$ increase by extracellular ATP in isolated rabbit renal proximal tubules. *Am J Physiol Cell Physiol* 270: C1096–C1104, 1996. doi:10.1152/ajpcell.1996.270.4.C1096.
61. **Constantinescu AR**, **Rozental R**, **Barac-Nieto M.** Age dependence of tolerance to anoxia and changes in cytosolic calcium in rabbit renal proximal tubules. *Pediatr Nephrol* 10: 606–612, 1996. doi:10.1007/s004670050171.
62. **McCarty NA**, **O'Neil RG.** Calcium-dependent control of volume regulation in renal proximal tubule cells: II. Roles of dihydropyridine-sensitive and -insensitive Ca^{2+} entry pathways. *J Membr Biol* 123: 161–170, 1991. doi:10.1007/BF01998086.
63. **Putney JW Jr**, **Ribeiro CM.** Signaling pathways between the plasma membrane and endoplasmic reticulum calcium stores. *Cell Mol Life Sci* 57: 1272–1286, 2000. doi:10.1007/pl00000765.
64. **Lambers TT**, **Bindels RJ**, **Hoenderop JG.** Coordinated control of renal Ca^{2+} handling. *Kidney Int* 69: 650–654, 2006. doi:10.1038/sj.ki.5000169.
65. **So CL**, **Meinert C**, **Xia Q**, **Robitaille M**, **Roberts-Thomson SJ**, **Monteith GR.** Increased matrix stiffness suppresses ATP-induced sustained Ca^{2+} influx in MDA-MB-231 breast cancer cells. *Cell Calcium* 104: 102569, 2022. doi:10.1016/j.ceca.2022.102569.
66. **Davies JE**, **Lopresto D**, **Apta BHR**, **Lin Z**, **Ma W**, **Harper MT.** Using Yoda-1 to mimic laminar flow in vitro: tool to simplify drug testing. *Biochem Pharmacol* 168: 473–480, 2019. doi:10.1016/j.bcp.2019.08.013.